Chapter 9
Modeling and Interaction of a Vehicle–Road System with Nonlinearity and Viscoelasticity

This chapter presents a nonlinear vehicle–road coupled model which is composed of a seven-degree-of-freedom (DOF) vehicle and a simply supported double-layer rectangular thin plate on a nonlinear viscoelastic foundation. The nonlinearity of the suspension stiffness, suspension damping, and tire stiffness is considered and the Leaderman constitutive relation and Burgers model are applied to describe the nonlinear and viscoelastic properties of the asphalt pavement material.

The equations of motion for the vehicle–road system are derived and the partial differential equation of the road pavement is discretized into an infinite number of second-order ordinary differential equations and first-order ordinary differential equations by Galerkin's method and a mathematical transform. A numerical integration method for solving this coupled system is developed and the nonlinear dynamic behaviors of the system are analyzed. In addition, the simulation results of the nonlinear viscoelastic model are compared to those of the linear or elastic model. The effects of system parameters on vehicle riding comfort and road damage are investigated [1, 2].

9.1 System Models and Equations of Motion

9.1.1 Modeling Nonlinearity and Viscoelasticity

A seven-DOF nonlinear vehicle and a double-layer rectangular thin plate on a nonlinear viscoelastic foundation with four simply supported boundaries are used to model the vehicle and the pavement. Figure 9.1 shows the nonlinear vehicle–road coupled system built in this work. In this model, the nonlinearity of tire and suspension and the viscoelasticity of pavement material are considered.

The nonlinear dynamic tire force can be formulated as

$$F_{tk} = k_t Z_t + \beta_1 k_t Z_t^2 + c_t \dot{Z}_t \tag{9.1}$$

© Science Press, Beijing and Springer-Verlag Berlin Heidelberg 2015

S. Yang et al., *Dynamics of Vehicle-Road Coupled System,*
DOI 10.1007/978-3-662-45957-7_9

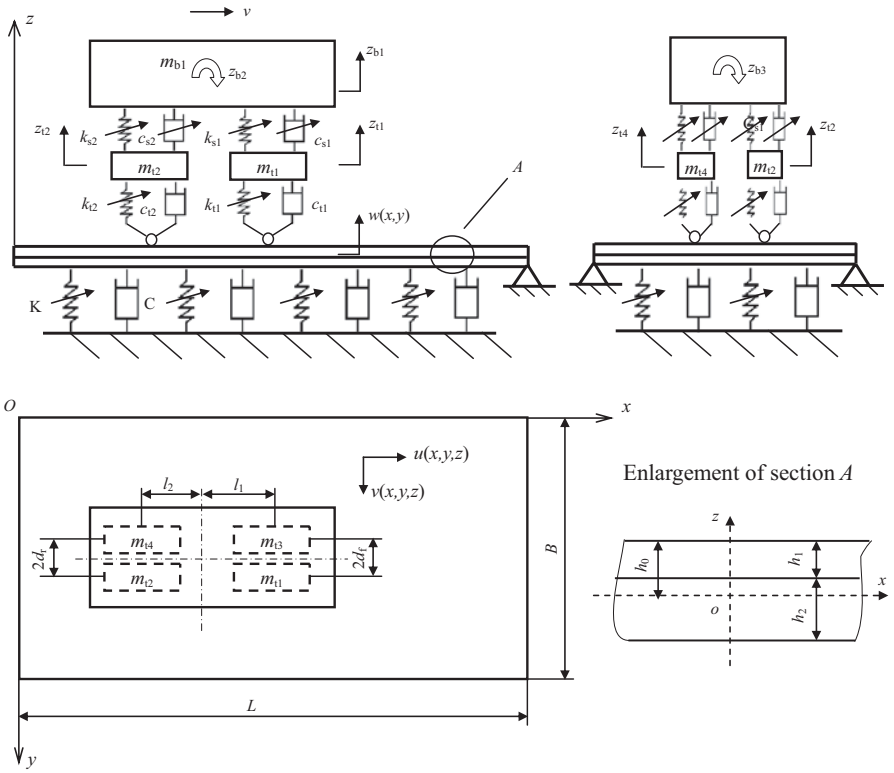

Fig. 9.1 The three-dimensional nonlinear vehicle–road coupled system. (Reprinted from [1], with kind permission from ASME)

where k_t is the linear tire stiffness, β_1 is the nonlinear tire stiffness coefficient, c_t is the tire damping coefficient, Z_t and $\dot{Z}_t$ are the relative vertical displacement and velocity between the wheel and the road surface, respectively.

The nonlinear spring force of the vehicle suspension is modeled as

$$F_{sk} = k_s z_s + \beta_2 k_s z_s^2 + \beta_3 k_s z_s^3 \tag{9.2}$$

where k_s is the linear stiffness coefficient of the suspension, β_2 and β_3 are the square and cubic nonlinear stiffness coefficients of the suspension, Z_s is the relative vertical displacement between the wheel and the vehicle body.

The hydraulic damper of the vehicle suspension is modeled as

$$F_{sc} = C_s(1+\beta_4 sig(\dot{Z}_s))\dot{Z}_s^{1.25} \tag{9.3}$$

where c_s is the linear damping coefficient of the suspension, β_4 is the asymmetry coefficient, $\dot{z}_s$ is the relative vertical velocity between the wheel and the vehicle body.

The upper and lower layers of the plate and the viscoelastic foundation stand for the asphalt topping, base course, and subgrade of the road, respectively. The Leaderman constitutive relation and the Burgers model are applied here to model the nonlinear viscous behaviors of the asphalt topping. The base course is assumed to be linear elastic. The Leaderman constitutive relation [3–5]can be expressed as

$$\begin{aligned}\sigma &= E_0(\varepsilon(x,z,t)+\beta_5\varepsilon(x,z,t)^2+\beta_6\varepsilon(x,z,t)^3)\\ &+\int_0^t \dot{E}(t-\tau)(\varepsilon(x,z,\tau)+\beta_4\varepsilon(x,z,\tau)^2+\beta_5\varepsilon(x,z,\tau)^3)d\tau\end{aligned} \tag{9.4}$$

where E_0 is the initial elastic modulus, β_5 is the square nonlinear coefficient, β_6 is the cubic nonlinear coefficient, and $E(t)$ is the relax function which is derived from the Burgers model for the asphalt mix. The Burgers model [6–8] is shown in Fig. 9.2 and can be written as

$$\sigma + p_1\dot{\sigma} + p_2\ddot{\sigma} = q_1\dot{\varepsilon} + q_2\ddot{\varepsilon} \tag{9.5}$$

where

$$\begin{aligned}p_1 &= \frac{\eta_2}{E_1}+\frac{\eta_2+\eta_3}{E_3},\\ p_2 &= \frac{\eta_2\eta_3}{E_1E_3},\\ q_1 &= \eta_2,\\ q_2 &= \frac{\eta_2\eta_3}{E_3}.\end{aligned} \tag{9.6}$$

The relax function obtained from Eq. (9.6) is

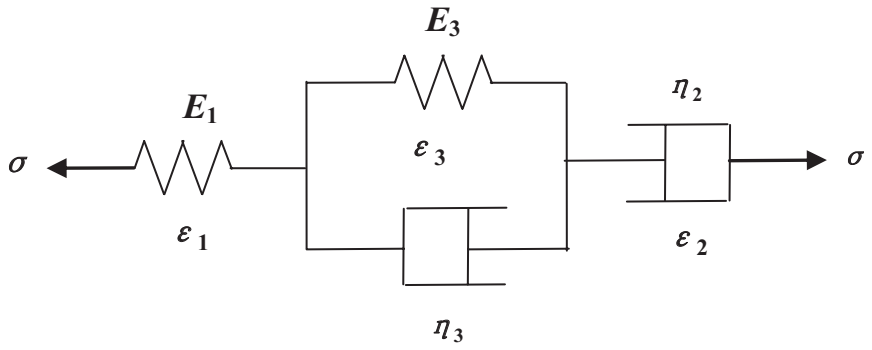

Fig. 9.2 The Burgers model. (Reprinted from [1], with kind permission from ASME)

$$E(t) = Ae^{-\alpha t} + Be^{-\beta t} \tag{9.7}$$

where

$$\begin{aligned} &\alpha = \frac{p_1 + \sqrt{p_1^2 - 4p_2}}{2p_2}, \beta = \frac{p_1 - \sqrt{p_1^2 - 4p_2}}{2p_2}, \\ &A = \frac{1}{\sqrt{p_1^2 - 4p_2}}(\alpha q_2 - q_1), B = \frac{1}{\sqrt{p_1^2 - 4p_2}}(q_1 - \beta q_2). \end{aligned} \tag{9.8}$$

The road subgrade is modeled by a nonlinear Kelvin foundation [9, 10] and the reaction force of the subgrade is

$$P = kZ_r + \beta_7 kz_r^3 + c\dot{z}_r \tag{9.9}$$

where K is the foundation response modulus, β_7 is the cubic nonlinear coefficient, and C is the foundation damping coefficient.

9.1.2 The Equations of Motion for a Nonlinear Vehicle

The vehicle equations of motion can be obtained by d'Alembert's principle

$$M_v\ddot{Z}_v + C_v\dot{Z}_v + K_vZ_v = R_v \tag{9.10}$$

where

$$M_v = diag[m_{b1} \quad m_{b2} \quad m_{b3} \quad m_{t1} \quad m_{t2} \quad m_{t3} \quad m_{t4}] \tag{9.11}$$

$$K_v = \begin{bmatrix} \sum_{i=1}^{4} k_{si} & -k_{s1}l_1 + k_{s2}l_2 - k_{s3}l_1 + k_{s4}l_2 & -k_{s1}d_f - k_{s2}d_r + k_{s3}d_f + k_{s4}d_r & -k_{s1} & -k_{s2} & -k_{s3} & -k_{s4} \\ & k_{s1}l_1^2 + k_{s2}l_2^2 + k_{s3}l_1^2 + k_{s4}l_2^2 & k_{s1}l_1d_f - k_{s2}l_2d_r - k_{s3}l_1d_f + k_{s4}l_2d_r & k_{s1}l_1 & -k_{s2}l_2 & k_{s3}l_1 & -k_{s4}l_2 \\ & & k_{s1}d_f^2 + k_{s2}d_r^2 + k_{s3}d_f^2 + k_{s4}d_r^2 & k_{s1}d_f & k_{s2}d_r & -k_{s3}d_f & -k_{s4}d_r \\ & & & k_{s1} & 0 & 0 & 0 \\ & & & & k_{s2} & 0 & 0 \\ & & & & & k_{s3} & 0 \\ & & & & & & k_{s4} \end{bmatrix} \tag{9.12}$$

$$C_v = \begin{bmatrix} \sum_{i=1}^{4} c_{si} & -c_{s1}l_1 + c_{s2}l_2 - c_{s3}l_1 + c_{s4}l_2 & -c_{s1}d_f - c_{s2}d_r + c_{s3}d_f + c_{s4}d_r & -c_{s1} & -c_{s2} & -c_{s3} & -c_{s4} \\ & c_{s1}l_1^2 + c_{s2}l_2^2 + c_{s3}l_1^2 + c_{s4}l_2^2 & c_{s1}l_1 d_f - c_{s2}l_2 d_r - c_{s3}l_1 d_f + c_{s4}l_2 d_r & c_{s1}l_1 & -c_{s2}l_2 & c_{s3}l_1 & -c_{s4}l_2 \\ & & c_{s1}d_f^2 + c_{s2}d_r^2 + c_{s3}d_f^2 + c_{s4}d_r^2 & c_{s1}d_f & c_{s2}d_r & -c_{s3}d_f & -c_{s4}d_r \\ & & & c_{s1} & 0 & 0 & 0 \\ & & & & c_{s2} & 0 & 0 \\ & & & & & c_{s3} & 0 \\ & & & & & & c_{s4} \end{bmatrix} \tag{9.13}$$

$$R_v = [0 \quad 0 \quad 0 \quad -F_{t1} \quad -F_{t2} \quad -F_{t3} \quad -F_{t4}]^T \tag{9.14}$$

$$Z_v = \begin{bmatrix} z_{b1} & z_{b2} & z_{b3} & z_{t1} & z_{t2} & z_{t3} & z_{t4} \end{bmatrix}^T. \tag{9.15}$$

z_{b1}, z_{b2}, and z_{b3} are the vehicle body's vertical, pitching, and rolling displacements respectively and $z_{t1}, z_{t2}, z_{t3}, z_{t4}$ are the wheel's vertical displacements. Furthermore, m_1 is the mass of the vehicle body, m_2 and m_3 are the moments of inertia of the vehicle body in the pitching and rolling directions respectively, and $m_{t1}, m_{t2}, m_{t3}, and\, m_{t4}$ are the wheels' masses. F_{t1}, F_{t2}, F_{t3}, and F_{t4} are the tire forces, which will be expressed by Eq. (9.56) in Sect. 9.1.4. d_f is half of the front wheel track, d_r is half of the rear wheel track, and $l_1 + l_2$ is the wheel space. $k_{ti}, k_{si}, c_{si} (i = 1 \sim 4)$ are equivalent nonlinear coefficients of the tire stiffness, suspension stiffness, and damping, which are expressed by

$$k_{ti} = k_{tli} + \beta_1 k_{tli}[Z_{ti} - r_{ti} - w(x_{ti}, y_{ti}, t)] \tag{9.16}$$

$$k_{si} = k_{sli} + \beta_2 k_{sli}(Z_{b1} - Z_{ti}) + \beta_3 k_{sli}(Z_{b1} - Z_{ti})^2 \tag{9.17}$$

$$c_{si} = c_{sli}(1 + \beta_4 sig(\dot{Z}_{b1} - \dot{Z}_{ti}) \left| \dot{Z}_{b1} - \dot{Z}_{ti} \right|^{0.25} \tag{9.18}$$

where $i = 1 \sim 4$, k_{tli}, k_{sli}, c_{sli} are linear coefficients of the stiffness or damping, r_{ti} and $w(x_{ti}, y_{ti}, t)$ are the road roughness and pavement displacements at the midpoint of the tire print.

9.1.3 The Equations of Motion for the Nonlinear and Viscoelastic Pavement

The directions of the vertical, longitudinal, and transverse pavement displacements are shown in Fig. 9.1. According to elastic dynamics [11, 12], the pavement displacements take the following form

$$\begin{cases} u(x,y,z,t) = -z\dfrac{\partial w}{\partial y} \\ v(x,y,z,t) = -z\dfrac{\partial w}{\partial y} \\ w(x,y,t) \quad = w(x,y,t) \end{cases} . \tag{9.19}$$

The relationship between the pavement strains and displacements is

$$\begin{cases} \varepsilon_x \ = -z\dfrac{\partial^2 w}{\partial x^2} \\ \varepsilon_y \ = -z\dfrac{\partial^2 w}{\partial y^2} \\ \gamma_{xy} = -2z\dfrac{\partial^2 w}{\partial x \partial y} \end{cases} . \tag{9.20}$$

With the Leaderman constitutive relation Eq. (9.4), the asphalt topping stresses can be written as

$$\begin{cases} \sigma_x = \dfrac{E_1}{1-\mu_1^2}[g_1(x,y,z,t) + \int_0^t \dfrac{E(t-\tau)}{E_1} g_1(x,y,z,\tau)d\tau] \\ \sigma_y = \dfrac{E_1}{1-\mu_1^2}[g_2(x,y,z,t) + \int_0^t \dfrac{E(t-\tau)}{E_1} g_2(x,y,z,\tau)d\tau] \\ \tau_{xy} = G_1(g_3(x,y,z,t) + \int_0^t \dfrac{E(t-\tau)}{G_1} g_3(x,y,z,\tau)d\tau) \end{cases} \tag{9.21}$$

where E_1, G_1, and μ_1 are the elastic modulus, the shear modulus, and Poisson's ratio of the asphalt pavement, respectively. The expressions of g_1, g_2, and g_3 are

$$\begin{aligned} g_1(x,y,z,t) = &-z\frac{\partial^2 w}{\partial x^2} + \beta_5 z^2 (\frac{\partial^2 w}{\partial x^2})^2 - \beta_6 z^3 (\frac{\partial^2 w}{\partial x^2})^3 \\ &+ \mu_1(-z\frac{\partial^2 w}{\partial y^2} + \beta_5 z^2 (\frac{\partial^2 w}{\partial y^2})^2 - \beta_6 z^3 (\frac{\partial^2 w}{\partial y^2})^3) \end{aligned} \tag{9.22}$$

$$\begin{aligned} g_2(x,y,z,t) = &-z\frac{\partial^2 w}{\partial y^2} + \beta_5 z^2 (\frac{\partial^2 w}{\partial y^2})^2 - \beta_6 z^3 (\frac{\partial^2 w}{\partial y^2})^3 \\ &+ \mu_1(-z\frac{\partial^2 w}{\partial x^2} + \beta_5 z^2 (\frac{\partial^2 w}{\partial x^2})^2 - \beta_6 z^3 (\frac{\partial^2 w}{\partial x^2})^3) \end{aligned} \tag{9.23}$$

$$g_3(x,y,z,t) = -2z\frac{\partial^2 w}{\partial x \partial y} + 4\beta_5 z^2 (\frac{\partial^2 w}{\partial x \partial y})^2 - 8\beta_6 z^3 (\frac{\partial^2 w}{\partial x \partial y})^3. \tag{9.24}$$

For the linear constitutive relation, the stresses of the base course are

$$\begin{cases} \sigma_x = -\dfrac{E_1}{1-\mu_2^2} z[\dfrac{\partial^2 w}{\partial x^2} + \mu_2 \dfrac{\partial^2 w}{\partial y^2}] \\ \sigma_y = -\dfrac{E_1}{1-\mu_2^2} z[\dfrac{\partial^2 w}{\partial y^2} + \mu_2 \dfrac{\partial^2 w}{\partial x^2}] \\ \tau_{xy} = -2G_2 z \dfrac{\partial^2 w}{\partial x \partial y} \end{cases} \tag{9.25}$$

where E_2, G_2, and μ_2 are the elastic modulus, the shear modulus, and Poisson's ratio of the base course, respectively.

The position of the stress-neutral layer is shown in Fig. 9.1 and has been determined in Chap. 5,

$$h_0 = \frac{E_1 h_1^2 + E_2(2h_1 + h_2)h_2}{2E_1 h_1 + 2E_2 h_2}. \tag{9.26}$$

The internal forces of the double-layer, thin plate satisfy the following equation

$$\begin{cases} M_x = \int_{h_0-h_1-h_2}^{h_0} \sigma_x z dz \\ = -D_{x1}\dfrac{\partial^2 w}{\partial x^2} - D_{x2}(\dfrac{\partial^2 w}{\partial x^2})^2 - D_{x3}(\dfrac{\partial^2 w}{\partial x^2})^3 - D_{y1}\dfrac{\partial^2 w}{\partial y^2} \\ \quad - D_{y2}(\dfrac{\partial^2 w}{\partial y^2})^2 - D_{y3}(\dfrac{\partial^2 w}{\partial y^2})^3 - \int_0^t E(t-\tau) D_{E1}(x,y,\tau) d\tau \\ M_y = \int_{h_0-h_1-h_2}^{h_0} \sigma_y z dz \\ = -D_{y1}\dfrac{\partial^2 w}{\partial x^2} - D_{y2}(\dfrac{\partial^2 w}{\partial x^2})^2 - D_{y3}(\dfrac{\partial^2 w}{\partial x^2})^3 - D_{x1}\dfrac{\partial^2 w}{\partial y^2} \\ \quad - D_{x2}(\dfrac{\partial^2 w}{\partial y^2})^2 - D_{x3}(\dfrac{\partial^2 w}{\partial y^2})^3 - \int_0^t E(t-\tau) D_{E2}(x,y,\tau) d\tau \\ M_{xy} = \int_{h_0-h_1-h_2}^{h_0} \tau_{xy} z dz = -D_{xy1}\dfrac{\partial^2 w}{\partial x \partial y} - D_{xy2}(\dfrac{\partial^2 w}{\partial x \partial y})^2 - D_{xy3}(\dfrac{\partial^2 w}{\partial x \partial y})^3 \\ \quad - \int_0^t E(t-\tau) D_{Exy}(x,y,\tau) d\tau \end{cases} \tag{9.27}$$

where

$$D_{x1} = \frac{h_1(h_1^2 E_1 - 3h_0 h_1 E_1 + 3h_0^2 E_1)}{3(1-\mu_1^2)} + \frac{E_2[(h_0-h_1)^3 - (h_0-h_1-h_2)^3]}{3(1-\mu_2^2)} \tag{9.28}$$

$$D_{x2} = \frac{h_1\beta_5 E_1(h_1^3 + 6h_0^2 h_1 - 4h_0 h_1^2 - 4h_0^3)}{4(1-\mu_1^2)} \tag{9.29}$$

$$D_{x3} = \frac{h_1\beta_6 E_1(-5h_0 h_1^3 + 10h_0^2 h_1^2 - 10h_0^3 h_1 + 5h_0^4 + h_1^4)}{5(1-\mu_1^2)} \tag{9.30}$$

$$D_{y1} = \frac{\mu_1 h_1(h_1^2 E_1 - 3h_0 h_1 E_1 + 3h_0^2 E_1)}{3(1-\mu_1^2)} + \frac{\mu_2 E_2[(h_0-h_1)^3 - (h_0-h_1-h_2)^3]}{3(1-\mu_2^2)} \tag{9.31}$$

$$D_{y2} = \frac{\mu_1 h_1\beta_5 E_1(h_1^3 + 6h_0^2 h_1 - 4h_0 h_1^2 - 4h_0^3)}{4(1-\mu_1^2)} \tag{9.32}$$

$$D_{y3} = \frac{\mu_1 h_1\beta_6 E_1(-5h_0 h_1^3 + 10h_0^2 h_1^2 - 10h_0^3 h_1 + 5h_0^4 + h_1^4)}{5(1-\mu_1^2)} \tag{9.33}$$

$$\begin{aligned} D_{xy1} = {} & -2G_1 h_1^2 h_0 + 2G_1 h_1 h_0^2 + \frac{2}{3}G_1 h_1^3 + 2G_2 h_0^2 h_2 - 4G_2 h_0 h_1 h_2 - 2G_2 h_0 h_2^2 \\ & + 2G_2 h_1^2 h_2 + 2G_2 h_1 h_2^2 + \frac{2}{3}G_2 h_2^3 \end{aligned} \tag{9.34}$$

$$D_{xy2} = G_1 h_1\beta_6(h_1^3 + 6h_0^2 h_1 - 4h_0 h_1^2 - 4h_0^3) \tag{9.35}$$

$$D_{xy3} = \frac{5}{8}G_1 h_1\beta_6(-5h_0 h_1^3 + 10h_0^2 h_1^2 - 10h_0^3 h_1 + 5h_0^4 + h_1^4) \tag{9.36}$$

$$D_{E1}(x,y,\tau) = -\int_{h_0-h_1}^{h_0} g_1(x,y,z,\tau)z/(1-\gamma_1^2)dz \tag{9.37}$$

$$D_{E2}(x,y,\tau) = -\int_{h_0-h_1}^{h_0} g_2(x,y,z,\tau)z/(1-\gamma_1^2)dz \tag{9.38}$$

$$D_{Exy}(x,y,\tau) = -\int_{h_0-h_1}^{h_0} g_3(x,y,z,\tau)zdz. \tag{9.39}$$

By integrating the three-dimensional balance equations of the double-layer, thin plate with the vertical-varied density along Z, one may obtain

$$\begin{cases} \dfrac{\partial M_x}{\partial x}+\dfrac{\partial M_{xy}}{\partial x}-Q_x=0 \\ \dfrac{\partial M_{xy}}{\partial x}+\dfrac{\partial M_y}{\partial y}-Q_y=0 \\ \dfrac{\partial Q_x}{\partial x}+\dfrac{\partial Q_y}{\partial y}-\rho h\dfrac{\partial^2 w}{\partial t^2}+q(x,y,t)=0 \end{cases} \tag{9.40}$$

where

$$\rho h=\int_{h_0-h_1}^{h_0}\rho_1 dz+\int_{h_0-h_1-h_2}^{h_0-h_1}\rho_2 dz=\rho_1 h_1+\rho_2 h_2. \tag{9.41}$$

From Eq. (9.40), one may obtain the partial differential equation of the pavement vertical vibration induced by the moving vehicle loads,

$$\begin{aligned} &D_{x1}(\frac{\partial^4 w}{\partial x^4}+\frac{\partial^4 w}{\partial y^4})+2(D_{y1}+2D_{xy1})\frac{\partial^4 w}{\partial x^2\partial y^2} \\ &+2D_{x2}[(\frac{\partial^3 w}{\partial x^3})^2+\frac{\partial^2 w}{\partial x^2}\frac{\partial^4 w}{\partial x^4}+(\frac{\partial^3 w}{\partial y^3})^2+\frac{\partial^2 w}{\partial y^2}\frac{\partial^4 w}{\partial y^4}] \\ &+2D_{y2}[(\frac{\partial^3 w}{\partial x\partial y^2})^2+\frac{\partial^2 w}{\partial y^2}\frac{\partial^4 w}{\partial x^2\partial y^2}+(\frac{\partial^3 w}{\partial x^2\partial y})^2+\frac{\partial^2 w}{\partial x^2}\frac{\partial^4 w}{\partial x^2\partial y^2}] \\ &+4D_{xy2}[\frac{\partial^3 w}{\partial x^2\partial y}\frac{\partial^3 w}{\partial x\partial y^2}+\frac{\partial^2 w}{\partial x\partial y}\frac{\partial^4 w}{\partial x^2\partial y^2}] \\ &+3D_{x3}[2\frac{\partial^2 w}{\partial x^2}(\frac{\partial^3 w}{\partial x^3})^2+2\frac{\partial^2 w}{\partial y^2}(\frac{\partial^3 w}{\partial y^3})^2+(\frac{\partial^2 w}{\partial x^2})^2\frac{\partial^4 w}{\partial x^4}+(\frac{\partial^2 w}{\partial y^2})^2\frac{\partial^4 w}{\partial y^4}] \\ &+3D_{y3}[2\frac{\partial^2 w}{\partial y^2}(\frac{\partial^3 w}{\partial x\partial y^2})^2+2\frac{\partial^2 w}{\partial x^2}(\frac{\partial^3 w}{\partial x^2\partial y})^2+(\frac{\partial^2 w}{\partial y^2})^2\frac{\partial^4 w}{\partial x^2\partial y^2} \\ &+(\frac{\partial^2 w}{\partial x^2})^2\frac{\partial^4 w}{\partial x^2\partial y^2}] \\ &+6D_{xy3}[2\frac{\partial^2 w}{\partial x\partial y}\frac{\partial^3 w}{\partial x\partial y^2}\frac{\partial^3 w}{\partial x^2\partial y}+(\frac{\partial^2 w}{\partial x\partial y})^2\frac{\partial^4 w}{\partial x^2\partial y^2}] \\ &+\int_0^t \dot{E}(t-\tau)(\frac{\partial^2 D_{E1}}{\partial x^2}+2\frac{\partial^2 D_{Exy}}{\partial x\partial y}+\frac{\partial^2 D_{E2}}{\partial y^2})d\tau \\ &+Kw+C\frac{\partial w}{\partial t}+\rho h\frac{\partial^2 w}{\partial t^2}=L(w)+\rho h\frac{\partial^2 w}{\partial t^2}=\sum_{s=1}^{4}F_{ts}\delta(x-x_{ts})\delta(y-y_{ts}) \end{aligned} \tag{9.42}$$

where F_{ts} is the s th tire force.

The displacement of the double-layer, thin plate with four simply supported boundaries can be expressed as

$$w(x,y,t)=\sum_{m=1}^{NM}\sum_{n=1}^{NN}U_{mn}(t)\sin\frac{m\pi x}{L}\sin\frac{n\pi y}{B}. \tag{9.43}$$

The substitution of Eq. (9.43) into Eq. (9.42) leads to a residual value. By limiting the residual value, the following equation can be obtained using Galerkin's method,

$$\int_0^L\int_0^B (L(w)+\rho h\frac{\partial^2 w}{\partial t^2}-\sum_{i=1}^{4}F_{ti}\delta(x-x_{ti})\delta(y-y_{ti}))\sin(i\pi x/L) \tag{9.44}$$
$$\sin(j\pi y/B)dxdy=0.$$

By simplifying the above equation, one can discretize Eq. (9.42) into a set of ordinary differential equations with an integral item,

$$M_{ij}\ddot{U}_{ij}+C_{ij}\dot{U}_{ij}+K_{1ij}U_{ij}+K_{2ij}U_{ij}^2+K_{3ij}U_{ij}^3+\int_0^t\dot{E}(t-\tau)G(\tau)d\tau=R_{ij} \tag{9.45}$$

where $i=1\sim NM$, $j=1\sim NN$,

$$M_{ij}=\frac{LB}{4}\rho h,\ C_{ij}=\frac{LB}{4}C, \tag{9.46}$$

$$K_{1ij}=D_{1ij}+\frac{LB}{4}K,K_{2ij}=D_{2ij},K_{3ij}=D_{3ij}+\frac{LB}{4}\beta_7 K \tag{9.47}$$

$$G(\tau)=\int_0^L\int_0^B(\frac{\partial^2 D_{E1}}{\partial x^2}+2\frac{\partial^2 D_{Exy}}{\partial x\partial y}+\frac{\partial^2 D_{E2}}{\partial y^2})\sin(i\pi x/L)\sin(j\pi y/B)dxdy \tag{9.48}$$
$$=A_{1ij}U_{ij}+A_{2ij}U_{ij}^2+A_{3ij}U_{ij}^3$$

$$R_{ij}=\int_0^L\int_0^B\sum_{s=1}^{4}F_{ts}\delta(x-x_{ts})\delta(y-y_{ts})\sin(i\pi x/L)\sin(j\pi y/B)dxdy \tag{9.49}$$

where D_{1ij}, D_{2ij}, D_{3ij}, A_{1ij}, A_{2ij}, and A_{3ij} are expressions of the system parameters.

Due to the integral term in Eq. (9.45), the following transformation [3–5] is applied,

$$x_{1ij}+x_{2ij}=\int_0^t\dot{E}(t-\tau)G(\tau)d\tau \tag{9.50}$$

By substituting Eq. (9.7) into Eq. (9.45), one obtains

$$\begin{cases} x_{1ij} = \int_0^t -A\alpha e^{-\alpha(t-\tau)} G(\tau) d\tau \\ x_{2ij} = \int_0^t -B\beta e^{-\beta(t-\tau)} G(\tau) d\tau \end{cases}. \tag{9.51}$$

The first derivation of Eq. (9.51) is

$$\begin{cases} \dot{x}_{1ij} = -\alpha x_{1ij} - A\alpha(A_{1ij}U_{ij} + A_{2ij}U_{ij}^2 + A_{3ij}U_{ij}^3) \\ x_{2ij} = -\beta x_{2ij} - B\beta(A_{1ij}U_{ij} + A_{2ij}U_{ij}^2 + A_{3ij}U_{ij}^3) \end{cases}. \tag{9.52}$$

The substitution of Eq. (9.50) into Eq. (9.45) leads to

$$M_{ij}\ddot{U}_{ij} + C_{ij}\dot{U}_{ij} + K_{1ij}U_{ij} + K_{2ij}U_{ij}^2 + K_{3ij}U_{ij}^3 + x_{1ij} + x_{2ij} = R_{ij}. \tag{9.53}$$

Thus Eq. (9.45) turns into one second-order ordinary differential equation, Eq. (9.53), and two first-order ordinary differential equations, Eq. (9.52). By re-writing them as matrix equations, one obtains

$$\begin{cases} \dot{X}_1 = -\alpha X_1 - A\alpha(A_1U + A_2U^2 + A_3U^3) = f(t, X_1, U) \\ \dot{X}_2 = -\beta X_2 - B\beta(A_1U + A_2U^2 + A_3U^3) = f(t, X_2, U) \end{cases} \tag{9.54}$$

$$M_r\ddot{U} + C_r\dot{U} + K_rU = R_r - X_1 - X_2 \tag{9.55}$$

where $\{X_1\}$, $\{X_2\}$, $\{AU\}$, $\{U\}$, and $\{R_f - X_1 - X_2\}$ are the column vectors with $NM \times NN$ lines. The components of these column vectors are x_{1ij}, x_{2ij}, $A_{1ij}U_{ij} + A_{2ij}U_{ij}^2 + A_{3ij}U_{ij}^3$, U_{ij}, and $R_{ij} - x_{1ij} - x_{2ij}$ respectively. The row subscript n_r of these column vectors depends on the mode numbers i and j through the expression $n_r = (i-1) \times NN + j$. $[M_r]$, $[C_r]$, and $[K_r]$ are square matrixes of order $NM \times NN$. Here, $K_r = [K_1 + K_2U + K_3U^2]$.

9.1.4 The Interaction Between the Vehicle and the Pavement

In regards to the coupling action of the vehicle and the road, the vertical contact force between the tire and the pavement is related not only to the tire motion and road surface roughness, but also to the road vibration. Based on Eq. (9.1), the vertical contact force between the tire and the pavement may be expressed as

$$F_{ts} = k_{ts}[x_{ts} - r_{ts} - w(x_{ts}, y_{ts}, t)] + c_{ts}[\dot{x}_{ts} - \dot{r}_{ts} - \frac{\partial w(x_{ts}, y_{ts}, t)}{\partial t}] \tag{9.56}$$

where $w(x_{ts}, y_{ts}, t)$ is the pavement displacement of the point under the s th tire and r_{ts} is the road surface roughness satisfying the following functions $r_{t1} = r_{t3} = B_0 \sin(\frac{2\pi vt}{L_0}),\quad r_{t2} = r_{t4} = B_0 \sin[\frac{2\pi}{L_0}(vt + l_1 + l_2)]$.

By substituting Eq. (9.43) into Eq. (9.56), one obtains

$$\begin{aligned} F_{ts} &= k_{ts}(z_{ts} - r_{ts}) + c_{ti}(\dot{z}_{ts} - \dot{r}_{ts}) - k_{ts}\sum_{m=1}^{NM}\sum_{n=1}^{NN} U_{mn}(t)\sin\frac{m\pi x}{L}\sin\frac{n\pi y}{B} \\ &-c_{ts}\sum_{m=1}^{NM}\sum_{n=1}^{NN}\dot{U}_{mn}(t)\sin\frac{m\pi x}{L}\sin\frac{n\pi y}{B} - c_{ts}\sum_{m=1}^{NM}\sum_{n=1}^{NN} U_{mn}(t)\frac{m\pi v}{L}\cos\frac{m\pi x}{L}\sin\frac{n\pi y}{B}. \end{aligned} \tag{9.57}$$

From Eq. (9.49) one may get

$$\begin{aligned} R_{ij} &= \int_0^L\int_0^B \sum_{s=1}^{4}[k_{ts}(z_{ts} - r_{ts}) + c_{ts}(\dot{z}_{ts} - \dot{r}_{ts}) - k_{ts}\sum_{m=1}^{NM}\sum_{n=1}^{NN} U_{mn}(t)\sin\frac{m\pi x}{L}\sin\frac{n\pi y}{B} \\ &-c_{ts}\sum_{m=1}^{NM}\sum_{n=1}^{NN}\dot{U}_{mn}(t)\sin\frac{m\pi x}{L}\sin\frac{n\pi y}{B} - c_{ts}\sum_{m=1}^{NM}\sum_{n=1}^{NN} U_{mn}(t)\frac{m\pi v}{L}\cos\frac{m\pi x}{L}\sin\frac{n\pi y}{B}] \\ &\delta(x - x_{ts})\delta(y - y_{ts})\sin(i\pi x/L)\sin(j\pi y/B)dxdy. \end{aligned} \tag{9.58}$$

It is clear from the above two equations that the contact forces between the tire and the road pavement are not only influenced by the wheel displacement, wheel velocity, and road roughness, but also by the pavement vibration mode's displacement and velocity. Thus, Z_{ts}, the four wheel displacements, are coupled with U_{mn}, the pavement vibration mode's displacements.

Equation (9.10) and Eq. (9.55) can be rewritten in the following form,

$$[M]\{\ddot{Z}\} + [C]\{\dot{Z}\} + [K]\{Z\} = \{R\} \tag{9.59}$$

where

$$[M] = \begin{bmatrix} M_v & 0 \\ 0 & M_r \end{bmatrix},\quad \{R\} = \begin{Bmatrix} R_v \\ R_r - X_1 - X_2 \end{Bmatrix} \tag{9.60}$$

The scheme of $[C]$ is

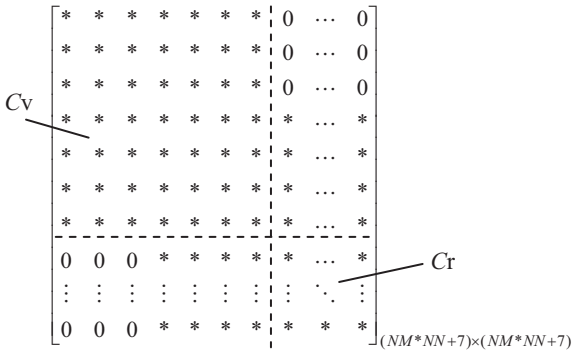

The scheme of [K] is

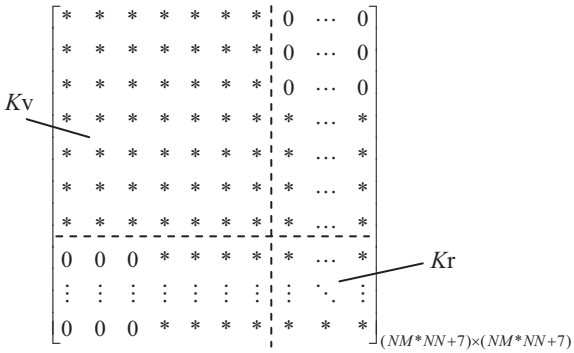

Consequently, Eq. (9.54) and Eq. (9.59) compose the first- and second-order ordinary differential equations of the nonlinear vehicle–road coupled system. Since the stiffness matrix K and damping matrix C of Eq. (9.59) have coupled items and time-varied parameters, the following numerical integration method is used to solve the equations.

9.2 Dynamic Responses of the Nonlinear Vehicle–Road Coupled System

The quick direct integral method and the Runge–Kutta method of order 4 can be combined to solve the system of equations. The routines of the calculation program in this study are as follows:

1. Establish the initial conditions

Assume the initial displacement and initial velocity of Eq. (9.59) are $\begin{cases}\{Z\}_0 = \{Z(0)\} \\ \{\dot{Z}\}_0 = \{\dot{Z}(0)\}\end{cases}$.

Assume the initial displacements of Eq. (9.54) are $\begin{cases}\{X_1\}_0 = \{X_1(0)\} \\ \{X_2\}_0 = \{X_2(0)\}\end{cases}$.

The initial acceleration can be obtained from Eq. (9.59),

$$\{\ddot{Z}\}_0 = [M]^{-1}(\{R\}_0 - [K]_0\{Z\}_0 - [C]_0\{\dot{Z}\}_0). \tag{9.61}$$

2. Compute the displacement, velocity, and acceleration of the vehicle–road coupled system when $t = (n+1)\Delta t$. Here, $n+1$ is the number of steps, and $n = 0,1,2,3\ldots$

Let $\phi = \psi = 0$ when $n = 0$ and $\phi = \psi = 1/2$ when $n \geq 1$. Given the integration time step Δt, one can build the following relations:

$$\begin{cases}\{Z\}_{n+1} = \{Z\}_n + \{\dot{Z}\}_n \Delta t + (1/2+\psi)\{\ddot{Z}\}_n \Delta t^2 - \psi\{\ddot{Z}\}_{n-1}\Delta t^2 \\ \{\dot{Z}\}_{n+1} = \{\dot{Z}\}_n + (1+\phi)\{\ddot{Z}\}_n \Delta t - \phi\{\ddot{Z}\}_{n-1}\Delta t\end{cases} \tag{9.62}$$

$$\begin{cases}\{X_1\}_{n+1} = \{X_1\}_n + \dfrac{\Delta t}{6}(f_{11} + 2f_{12} + 2f_{13} + f_{14}) \\ \{X_2\}_{n+1} = \{X_2\}_n + \dfrac{\Delta t}{6}(f_{21} + 2f_{22} + 2f_{23} + f_{24})\end{cases} \tag{9.63}$$

where

$$\begin{aligned}
&f_{11} = f_1(t_n, X_{1n}, U_n), f_{12} = f_1\left(t_n + \frac{\Delta t}{2}, X_{1n} + \frac{\Delta t}{2} f_{11}, U_n\right), \\
&f_{13} = f_1\left(t_n + \frac{\Delta t}{2}, X_{1n} + \frac{\Delta t}{2} f_{12}, U_n\right), f_{14} = f_1(t_n + \Delta t, X_{1n} + \Delta t f_{13}, U_n) \\
&f_{21} = f_2(t_n, X_{1n}, U_n), f_{22} = f_2\left(t_n + \frac{\Delta t}{2}, X_{1n} + \frac{\Delta t}{2} f_{21}, U_n\right), \\
&f_{23} = f_2\left(t_n + \frac{\Delta t}{2}, X_{1n} + \frac{\Delta t}{2} f_{22}, U_n\right), f_{24} = f_2(t_n + \Delta t, X_{1n} + \Delta t f_{23}, U_n).
\end{aligned} \tag{9.64}$$

By substituting Eq. (9.62) and Eq. (9.63) into Eq. (9.59) when $t = (n+1)\Delta t$, one can obtain

$$\begin{aligned}
\{\ddot{Z}\}_{n+1} = [M]^{-1}(&\{R\}_{n+1} - [K]_{n+1}\{Z\}_n - ([C]_{n+1} + [K]_{n+1}\Delta t)\{\dot{Z}\}_n \\
&- \{(1+\phi)[C]_{n+1} + (1/2+\psi)[K]_{n+1}\Delta t\}\{\ddot{Z}\}_n \Delta t \\
&+ (\phi[C]_{n+1} + \psi[K]_{n+1}\Delta t)\{A\}_{n-1}\Delta t.
\end{aligned} \tag{9.65}$$

3. By repeating process (2), one can get the displacement, velocity, and acceleration of the system step by step.

The convergence criterion of this method is

$$\Delta t < 2/\omega \text{ when } \quad \phi = \psi = 1/2 \, fa \tag{9.66}$$

where Δt is the integration time step, and ω is the natural angular frequency of the system.

During the dynamic simulation, the vehicle parameters correspond to those of a heavy truck. Parameters for the vehicle system are as follows [12, 13]:

$m_b1 = 15280$ kg, $m_b2 = 3 \times 10^5$ kg m^2, $m_b3 = 0.6 \times 10^5$ kg m^2, $m_t1 = m_t3 = 190$ kg, $m_t2 = m_t4 = 380$ kg, $k_{sl}1 = k_{sl}3 = 370 \times 10^3$ N/m, $k_{sl}2 = k_{sl}4 = 920 \times 10^3$ N/m, $c_{sl}1 = c_{sl}3 = 12{,}000$ N s/m, $c_{sl}2 = c_{sl}4 = 30{,}000$ N s/m, $k_{tl}1 = k_{tl}3 = 0.73 \times 10^6$ N/m, $k_{tl}2 = k_{tl}4 = 1.46 \times 10^6$ N/m, $c_t1 = c_t3 = 600$ N s/m, $c_t2 = c_t4 = 900$ N s/m, $l_1 = 3.29$ m, $l_2 = 1.48$ m, $l_f = 1.90$ m, $l_r = 1.80$ m, $\beta_1 = 0.01$, $\beta_2 = 0.1$, $\beta_3 = 0.6$, $\beta_4 = 1/3$.

Parameters of the pavement and foundation are given below [14, 15]:

$L = 600$ m, $B = 24$ m, $h_1 = 0.09$ m, $E_1 = 2400$ MPa, $E_3 = 2400$ MPa, $\eta_2 = 3159.32$ MPa s, $\eta_3 = 509.61$ MPa s, $\mu_1 = 0.35$, $\rho_1 = 2.613 \times 10^3$ kg/m^3, $h_2 = 0.2$ m, $E_2 = 1100$ MPa, $\mu_2 = 0.35$, $\rho_2 = 2.083 \times 10^3$ kg/m^3, $K = 48 \times 10^6$ N/m^2, $C = 0.3 \times 10^4$ N s/m^2, $\beta_5 = 0.1$, $\beta_6 = 0.1$, $\beta_7 = 0.01$, $L_0 = 2.3$ m, $B_0 = 0.002$ m.

In order to confirm the validity of the integration results, two numerical tests were done to choose a suitable mode number for the pavement displacement and an integration time step. It is found that, when the time step is smaller than 1 ms and the mode number of the pavement is larger than 10, dynamic responses of the system vary slightly. Thus, a suitable value of NM is 10 and a suitable value of Δt is 1 ms.

The natural frequencies of the derived system are calculated with the system parameters selected above. The vertical, pitching, and rolling natural frequencies of the vehicle body and the vertical natural frequencies of the four wheels are 1.6314, 0.8076, 0.7562, 12.1137, 12.1357, 12.6053, and 12.6492 Hz, respectively. The natural frequencies of the road range from 34.1739 to 143.3673 Hz. By substituting the highest natural frequency of the coupled system 143.3673 Hz into Eq. (9.66), one obtains $\Delta t < 2/(2\pi \times 143.3673) = 2.2\text{ms}$. Because the time step Δt is 1 ms, the convergence criterion is well satisfied.

In addition, the responses that occur during the first 5 s are removed so as to minimize the effect of the transitional course. When $v = 10$ m/s and $B_0 = 0.002$ m, the time history of the vehicle body's vertical acceleration, phase trajectories, and Poincaré maps of the vehicle body's vertical motion, along with the power spectrum of the vehicle body's vertical displacement can be obtained, as shown in Fig. 9.3. From Fig. 9.3, it can be seen that the time history is periodic, the phase trajectories are a closed curve, the Poincaré map is a point, and the power spectrum consists of discrete lines. Thus it can be concluded that the vertical motion of the vehicle body is periodic. It has also been found that the peak frequencies in the power spectrum include 4.38, 8.73, 13.1, and 1.6 Hz, which correspond to one time, two times, and

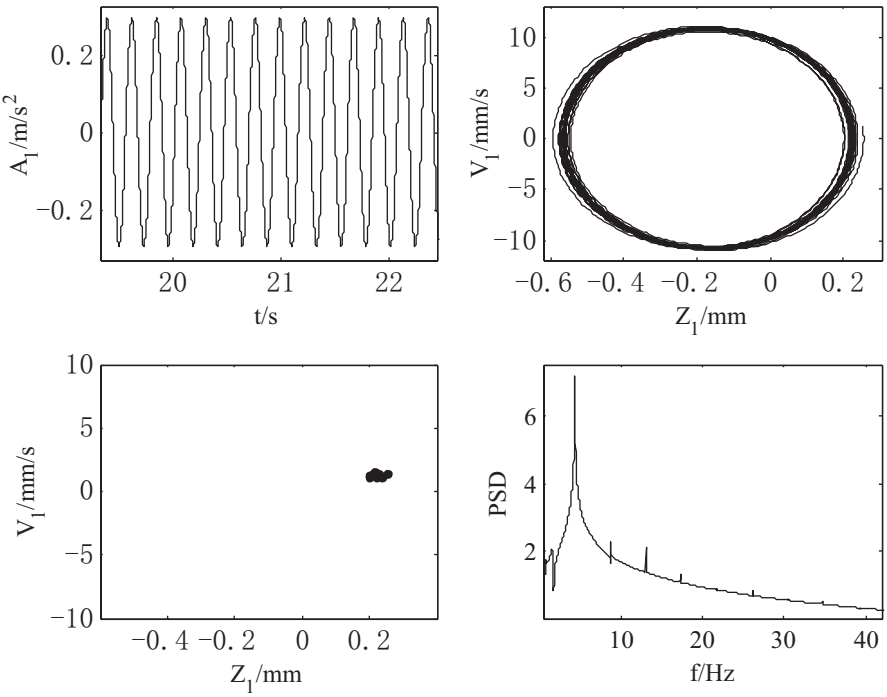

Fig. 9.3 Vehicle responses with B_0=0.002 m. (Reprinted from [1], with kind permission from ASME)

three times the road roughness excitation frequency, as well as the vertical natural frequency of the vehicle body respectively. The 4.38 and 1.6 Hz values may be easily explained using vibration theory: the frequency components of forced vibration include the excitation frequency and natural frequency of the system. The 8.73 and 13.1 Hz values may be the result of the square and cubic nonlinearities of the system, which result in two and three times the excitation frequency, respectively.

Figure 9.4 shows the time history, phase trajectories, Poincaré maps, and power spectrum of the pavement vertical displacement when B_0=0.002 m. It may be observed from Fig. 9.4 that the time history is not periodic, the phase trajectories are complicate and irregular, the Poincaré map is an unclosed curve, and the power spectrum consists of discrete lines. According to nonlinear vibration theory, the largest Lyapunov exponent may be used as a criterion for motion type. If the largest Lyapunov exponent is larger than zero, the system motion is possibly chaotic. On the other hand, if the largest Lyapunov exponent is zero, the system will have a periodic or quasiperiodic motion. When B_0=0.002 m, the largest Lyapunov exponent of the pavement displacement is computed using the method of Wolf [16, 17], and the result is zero. Thus it may be concluded that the vertical motion of the pavement is quasiperiodic. It is also found that the spectral peak frequencies are 4.38, 8.73, and 13.1 Hz, corresponding to one time, two times, and three times the road excitation

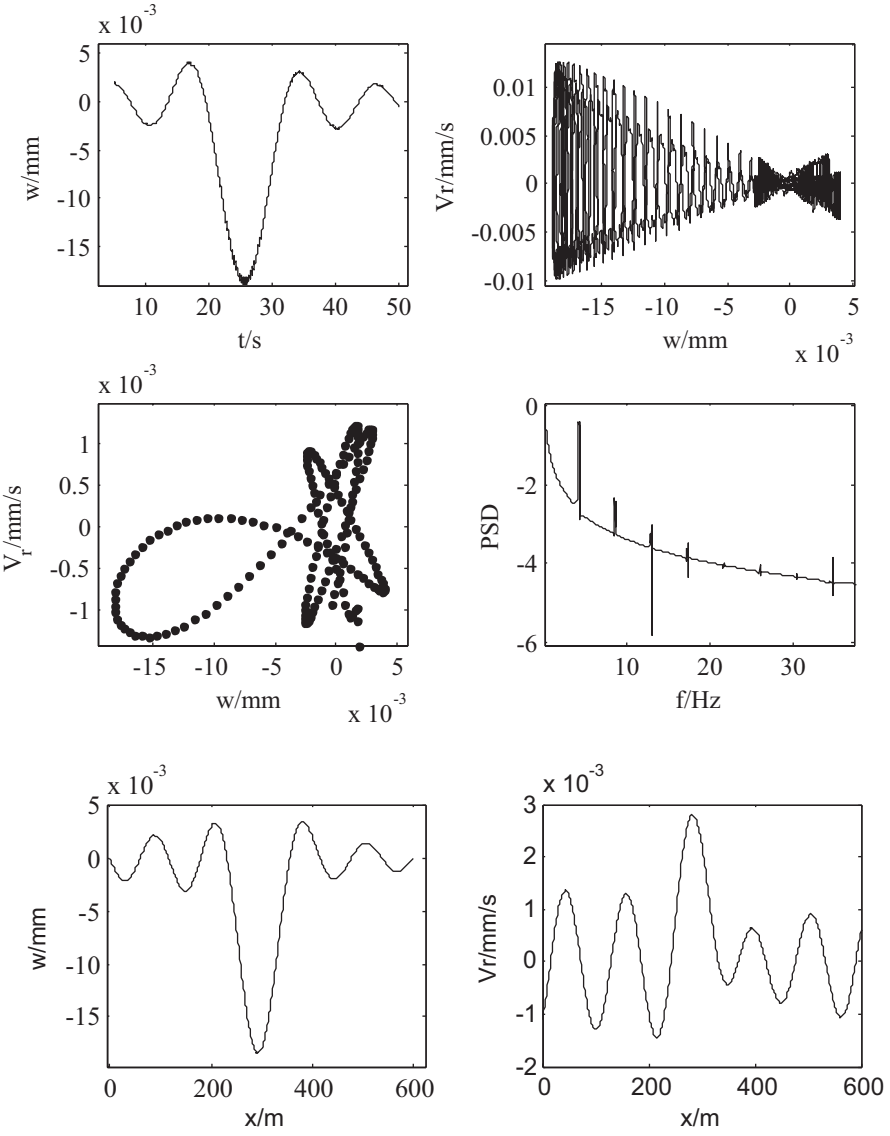

Fig. 9.4 Pavement responses with B_0=0.002 m. (Reprinted from [1], with kind permission from ASME)

frequency, respectively. Similarly, the square and cubic nonlinearity of the system cause the existence of two and three times the excitation frequency.

The dynamic responses of the vehicle body and the pavement in a vertical direction when B_0=0.02 and 0.1 m are also simulated. It is found that the vertical motion of the vehicle body is always periodic in all three cases, but the vertical motion of

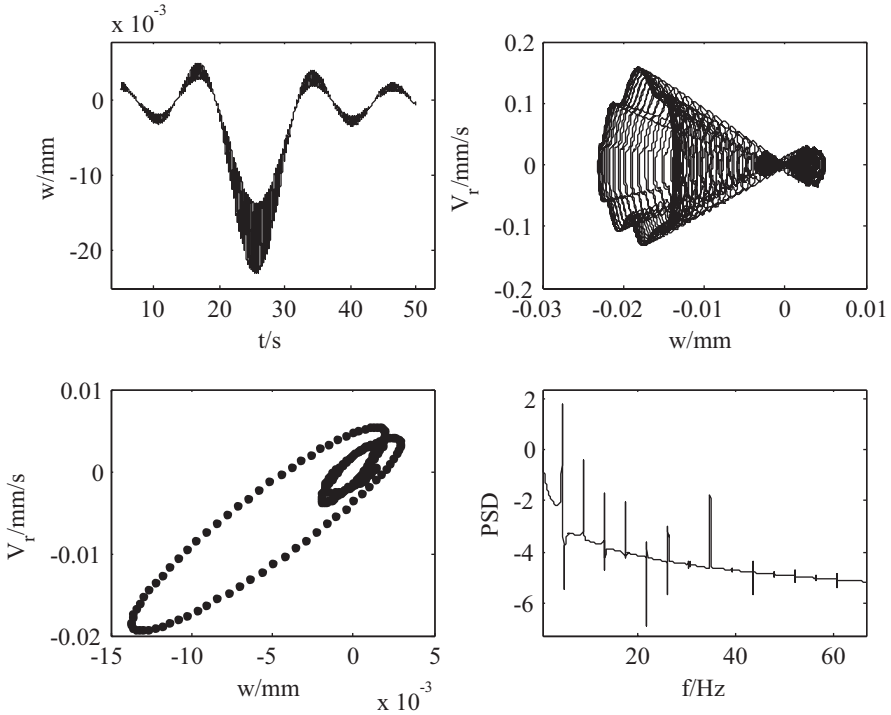

Fig. 9.5 Pavement responses with B_0=0.02 m. (Reprinted from [1], with kind permission from ASME)

the pavement is different in the three cases. Figures 9.5 and 9.6 show the pavement responses in the three cases.

It can be seen from the above two figures that

1. When B_0=0.02 m, the time history of the pavement vertical displacement is similar to that of when B_0=0.002 m. An exception is the appearance of a high-frequency wave. Then, the Poincaré map is a closed curve, and the power spectrum consists of more peaks than when B_0=0.002 m.
2. When B_0=0.1 m, the time history and phase trajectories of the pavement vertical motion are complicated and irregular, the Poincaré map looks like a narrow band, and the power spectrum consists not only of many peaks, but also of continuous broadband stochastic curves.

The largest Lyapunov exponents corresponding to these two cases (B_0=0.02 m, 0.1 m) are also computed and found to be 0 and 0.1912. Hence it may be concluded that the vertical motion of the pavement when B_0=0.02 m is quasiperiodic and the vertical motion of the pavement when B_0=0.1 m is chaotic.

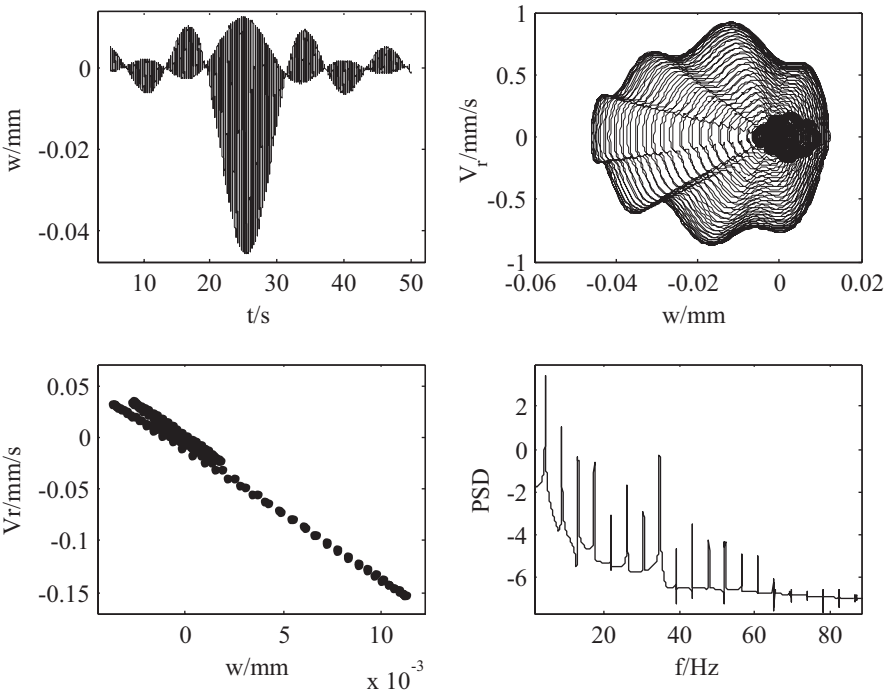

Fig. 9.6 Pavement responses with $B_0 = 0.1$ m

9.3 The Effects of Nonlinearity and Viscoelasticity on Vehicle and Road Responses

To investigate the effect of nonlinearity on vehicle and pavement responses, the amplitude–frequency response curves of the vehicle body's vertical acceleration and the pavement vertical displacement for a linear and nonlinear system are drawn, as shown in Fig. 9.7. In order to obtain a frequency range from 0.5 to 40 Hz, the wave length L_0 varies from 0.5 to 40 m, and the vehicle velocity V is set to 20 m/s. From Fig. 9.7 it can be seen that the effect of nonlinearity on the vehicle body vertical acceleration is greater than the effect on the pavement vertical displacement. At lower frequencies, the responses of the nonlinear system are larger than those of the linear system. However, in higher frequencies, the responses of the nonlinear system are smaller than that of the linear system.

In addition, Fig. 9.8 compares the amplitude–frequency response curves of the vehicle body vertical acceleration and the pavement vertical displacement for the linear elastic and viscoelastic asphalt topping. It may be observed from Fig. 9.8 that the effect of the viscoelastic pavement material on the vehicle response is much smaller than its effect on the pavement response. The response of the pavement with the viscoelastic material is greater than the response of the pavement with the linear elastic material.

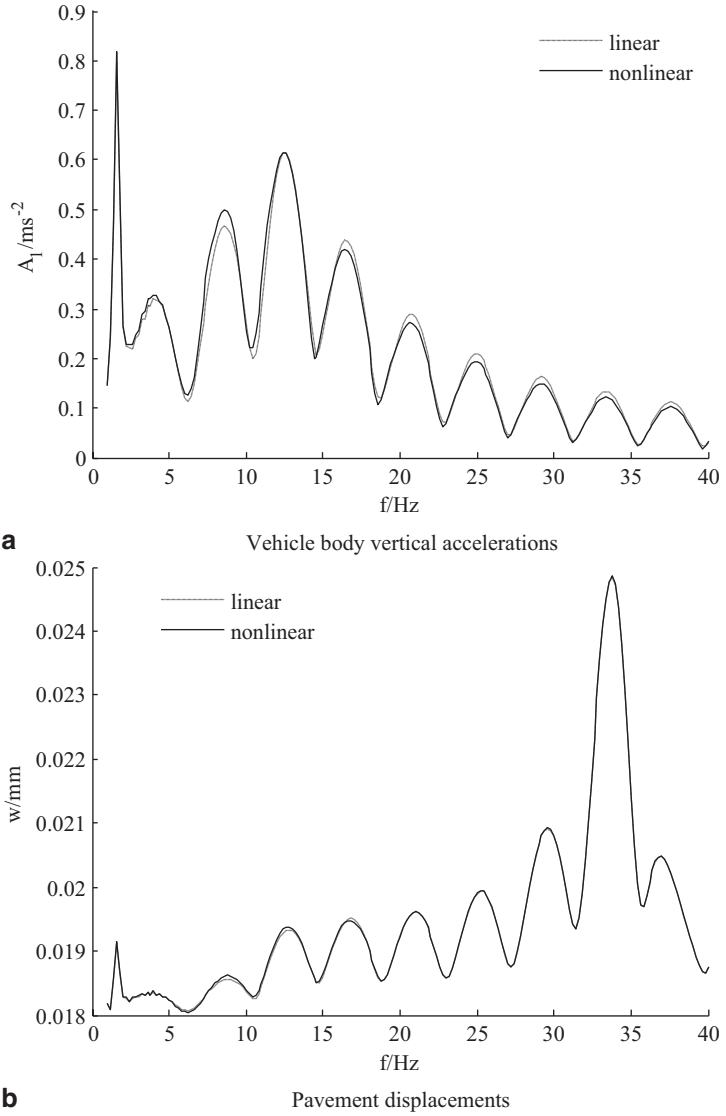

Fig. 9.7 The effect of nonlinearity on amplitude–frequency responses. **a** Vehicle body vertical accelerations. **b** Pavement displacements. (Reprinted from [1], with kind permission from ASME)

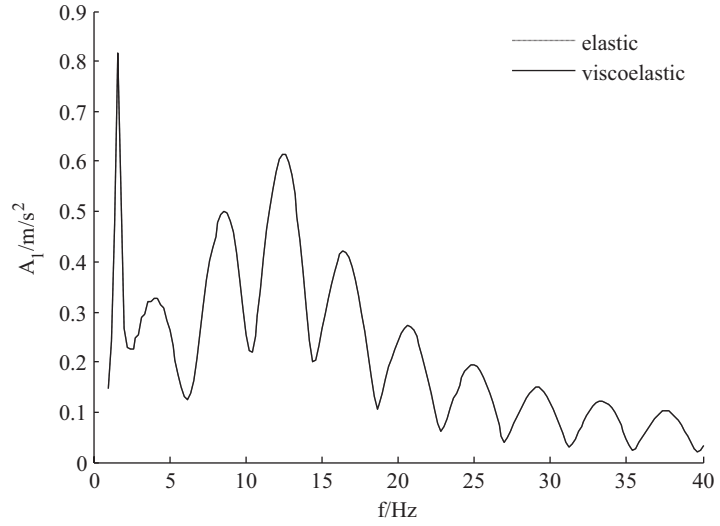

a Vehicle body vertical accelerations

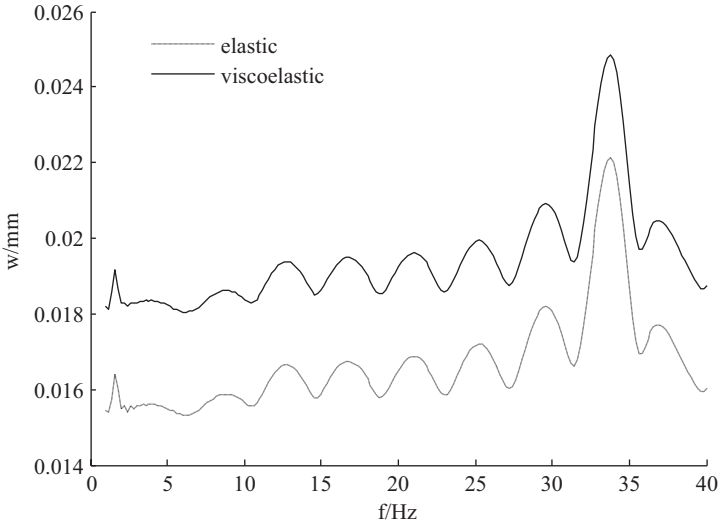

b Pavement displacements

Fig. 9.8 The effect of viscoelasticity on amplitude–frequency responses. **a** Vehicle body vertical accelerations. **b** Pavement displacements. (Reprinted from [1], with kind permission from ASME)

The effects of seven nonlinear parameters β_1, β_2, β_3, β_4, β_5, β_6, β_7, and four viscoelastic parameters E_1, E_3, η_2, η_3 on the vehicle body vertical acceleration, and the pavement displacement are studied, as shown in Fig. 9.9, 9.10, 9.11, 9.12, 9.13, 9.14, 9.15, 9.16, 9.17, 9.18, and 9.19. The main conclusions are listed here,

1. In four of the nonlinear parameters of the vehicle system, the effect of the suspension damper asymmetry coefficient β_4 is the greatest, the effects of the square nonlinear tire stiffness β_1 and the square nonlinear suspension stiffness β_2 are the second, and the effect of the cubic nonlinear suspension stiffness β_3 is the least. A large β_1 or small β_4 both benefit vehicle riding comfort and road service life. Small β_2 may improve vehicle riding comfort but hardly influences the pavement displacement.
2. The effects of the pavement nonlinear parameters β_5, β_6, and β_7 on the responses of the vehicle and pavement is very small. Therefore, these three nonlinear parameters may be omitted in order to simplify the calculations.
3. In four of the viscoelastic parameters of the pavement asphalt topping, the effect of E_1 on system response is greater than that of E_3, and the effect of η_2 on system response is greater than that of η_3. A small E_1, large E_3, large η_2, or large η_3 may not only improve vehicle riding comfort but also extend road service life.

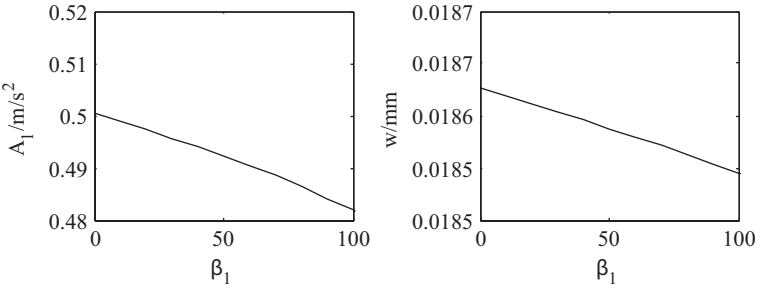

Fig. 9.9 The effect of square nonlinear tire stiffness β_1. (Reprinted from [2], with kind permission from Academy Publisher)

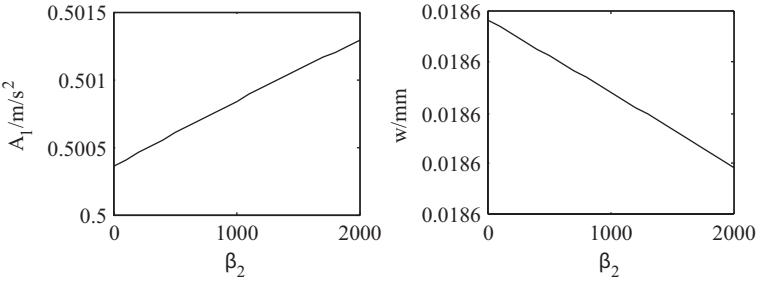

Fig. 9.10 The effect of square nonlinear suspension stiffness β_2. (Reprinted from [2], with kind permission from Academy Publisher)

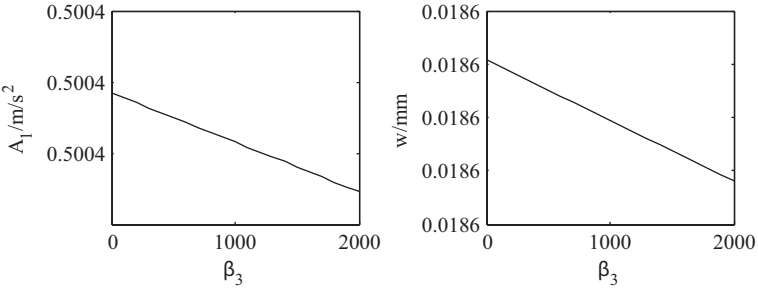

Fig. 9.11 The effect of cubic nonlinear suspension stiffness β_3. (Reprinted from [2], with kind permission from Academy Publisher)

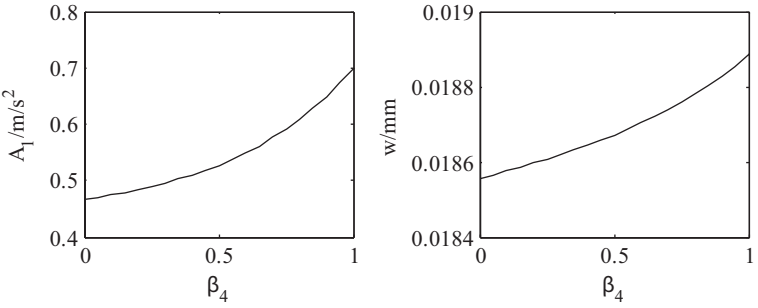

Fig. 9.12 The effect of suspension damper asymmetry coefficient β_4. (Reprinted from [2], with kind permission from Academy Publisher)

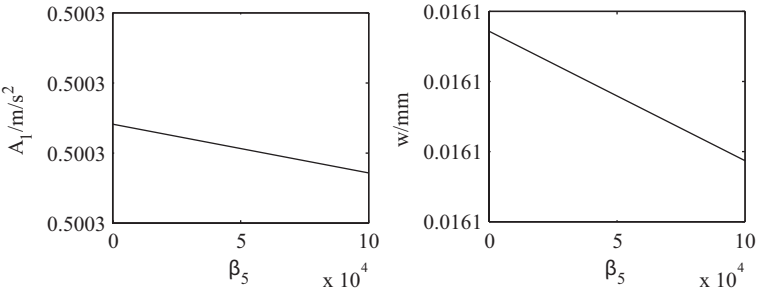

Fig. 9.13 The effect of square nonlinear pavement topping elastic β_5. (Reprinted from [2], with kind permission from Academy Publisher)

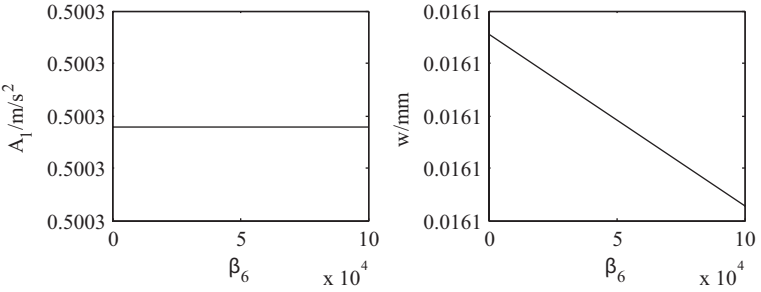

Fig. 9.14 The effect of cubic nonlinear pavement topping elastic β_6. (Reprinted from [2], with kind permission from Academy Publisher)

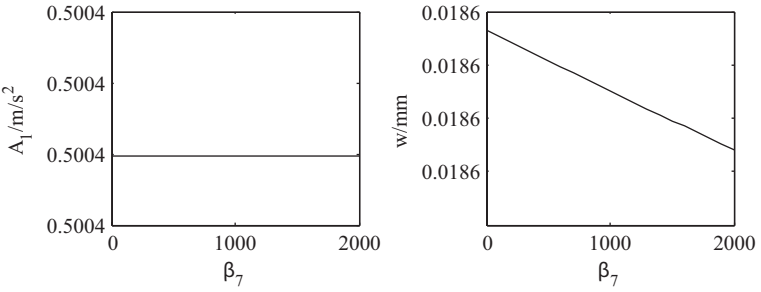

Fig. 9.15 The effect of nonlinear foundation stiffness β_7. (Reprinted from [2], with kind permission from Academy Publisher)

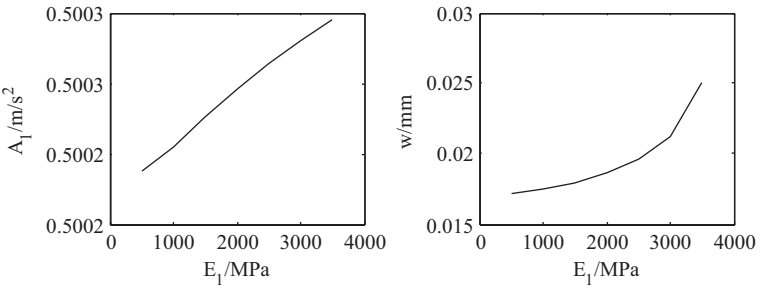

Fig. 9.16 The effect of pavement topping elastic modulus E_1. (Reprinted from [2], with kind permission from Academy Publisher)

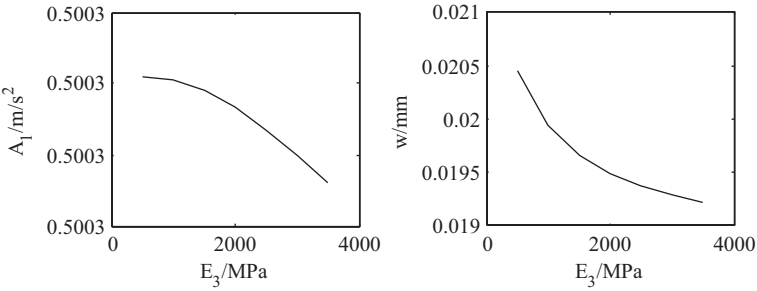

Fig. 9.17 The effect of pavement topping elastic modulus E_3. (Reprinted from [2], with kind permission from Academy Publisher)

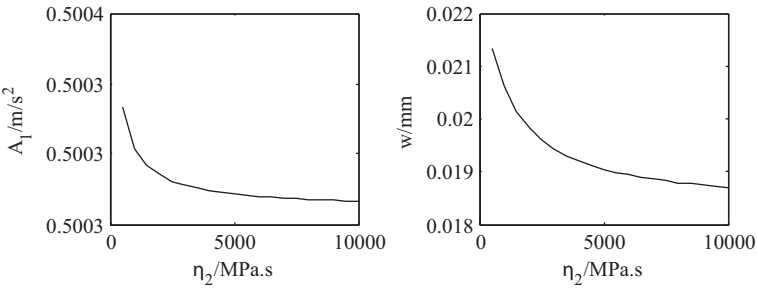

Fig. 9.18 The effect of pavement topping damping η_2. (Reprinted from [2], with kind permission from Academy Publisher)

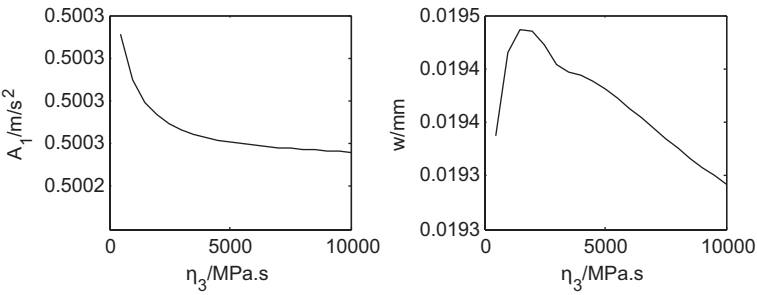

Fig. 9.19 The effect of pavement topping damping η_3. (Reprinted from [2], with kind permission from Academy Publisher)

9.4 Chapter Summary

In this chapter, a 3D vehicle–road coupled system with nonlinearity and viscoelasticity is built and the nonlinear responses of the vehicle and road are computed simultaneously. The effects of the nonlinear and viscous parameters on vehicle riding comfort and road damage are also analyzed. It can be found that

1. The effect of nonlinearity on the vehicle body vertical acceleration is greater than the effect on the pavement vertical displacement. At lower frequencies, the responses of the nonlinear system are greater than those of the linear system. However, at higher frequencies, the responses of the nonlinear system are smaller than those of the linear system. Hence, it is necessary to take into account the nonlinearity of the vehicle suspension to research the nonlinear dynamic phenomena of the vehicle and to improve computational accuracy. On the other hand, the nonlinearity of the pavement material may be neglected if one calculates only the amplitude of the pavement response.
2. The influence of the viscoelastic pavement material on the vehicle response is much smaller than that on the pavement response. The response of the pavement with viscoelastic asphalt topping is greater than the response with linear elastic material. Thus, the viscoelastic characteristic of asphalt topping should be considered in order to estimate the pavement response more accurately.

References

1. Li SH, Yang SP, Chen LQ. A nonlinear vehicle-road coupled model for dynamics research. J Comput Nonlinear Dyn. 2013;8(2):1–14.
2. Li SH, Lu YJ, Li HY. Effects of parameters on dynamics of a nonlinear vehicle-road coupled system. J Comput. 2011;6(12):2656–61.
3. Chen LQ, Cheng CJ, Zhang NH. Chaotic motion of viscoelastic beams with geometric and physical nonlinearities. Eng Mech. 2001;18(1):1–6.
4. Chen LQ, Cheng CJ. Dynamical behavior of nonlinear viscoelastic beams. Appl Math Mech. 2000;21(9):897–902.
5. Potapov VD, Marasanov AY. The investigation of the stability of elastic and viscoelastic rods under a stochastic excitation. Int J Solids Struct. 1997;34(11):1367–77.
6. Marynowski K, Kapitaniak T. Kelvin-Voigt versus burgers internal damping in modeling of axiallymoving viscoelastic web. Int J Non-linear Mech. 2002;37:1147–61.
7. Zheng JL. Application of Burgers model to the analysis of fatigue characteristic of bituminous mixtures. J Changsha Commun Inst. 1995;11(3):32–42.
8. Feng JL, Huang XM. Study on the method of determining viscoelastic parameters of asphalt binder. J Highw Transp Res Dev. 2006;23(5):16–22.
9. Qiu P, Wang XZ, Ye KY. Bifurcation and chaos of the circular plates on the nonlinear elastic foundation. Appl Math Mech. 2003;24(8):779–84.
10. Yang ZA, Zhao XJ, Xi XY. Nonlinear vibration and singularities analysis of a thin rectangular plate on a nonlinear elastic foundation. J Vib Shock. 2006;25(5):69–73.
11. Cao ZY. A Nonlinear dynamic analysis of functionally graded material plates. Acta Mech Solida Sin. 2006;27(1):21–5.
12. Cao ZY. Vibration theory of plates and shells [M]. Beijing: China Railway Press; 1989.

13. Xu B., Shi YB, Wang GD. Suspension non-linear components influence upon ride comfort and road friendliness. Veh Power Technol. 2005;1:46–51.
14. Chen J. A basic study on the interaction between vehicle and roadway [D]. Changchun: Jilin University, 2002.
15. Ke JP, Ding P. A study on the stress relaxation performance of an asphalt mixture. Highw Automot Appl. 2004;4:64–6.
16. Hu HY. Applied nonlinear dynamics. Beijing: Aero Industrial Press, 2000.
17. Wolf A, et al. Determining Lyapunov exponents from a time series. Physica D. 1985;16:285–317.